Molecular Catalysis

Benzyl Alcohol to Benzaldehyde Oxidation on MnOx Clusters: Unraveling Atomistic Features

Asynch.CoverPage.ManuscriptDraft

Common.Text.ManuscriptNumber:	MOLCAA-D-21-00373R1
Common.Labels.ArticleType	Research Paper
Common.Text.SectionCategory:	Computational heterogeneous catalysis
Common.SubmissionDetails.Keywords:	MnOx based catalysts; oxidative dehydrogenation; Catalyst Deactivation; reaction mechanisms; DFT
Common.SubmissionDetails.CorrespondingAuthor:	Dario Duca, D.Sc. Palermo, ITALY
Common.SubmissionDetails.FirstAuthor:	Laura Gueci
Common.SubmissionDetails.OrderOfAuthors:	Laura Gueci
	Francesco Ferrante, Prof.
	Antonio Prestianni, Dr.
	Francesco Arena, Prof.
	Dario Duca, Prof.
Common.SubmissionDetails.Abstract:	The catalytic oxidation of benzyl alcohol with O 2 is a promising option for the production of benzaldehyde, from both environmental and economical viewpoints. In particular, highly dispersed MnO x systems feature good activity and selectivity in a wide range of temperatures, although deactivation phenomena by over-oxidation and/or poisoning of active sites are generally recorded. On this account, a density functional theory study was performed on cluster-sized catalyst models, namely Mn 4 O 8 and over-oxygenated Mn 4 O 9 fragments, to predict the reactivity pattern of MnO x catalysts in the selective aerobic oxidation of benzyl alcohol. Several pathways concur to determine the whole reaction process and all of them were compared to unveil the atomistic details of the alcohol oxidation mechanism. Moreover, assuming that the consecutive formation of benzoic acid affects the activity-stability pattern of the MnO x based catalyst, also the benzaldehyde oxidation mechanism was computationally addressed. A systematic comparison of the benzyl alcohol and benzaldehyde oxidation mechanisms on the Mn 4 O 8 and Mn 4 O 9 fragments reveals some experimental strategies to test the reaction mechanisms and design alternative catalytic routes to decrease undesired parasitic reactions leading to catalyst deactivation. The matching structural, energetic and kinetic data are published in the Data in Brief journal [1].

Graphical Abstract

Benzyl Alcohol to Benzaldehyde Oxidation on MnO_x Clusters: Unraveling Atomistic Features

Laura Gueci, Francesco Ferrante, Antonio Prestianni, Francesco Arena, Dario Duca

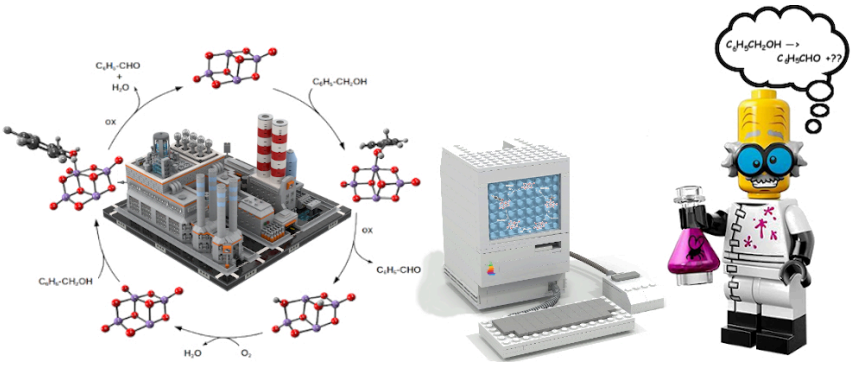

Highlights

Benzyl Alcohol to Benzaldehyde Oxidation on MnO_x Clusters: Unraveling Atomistic Features

Laura Gueci, Francesco Ferrante, Antonio Prestianni, Francesco Arena, Dario Duca

- Catalytic oxidation of benzyl alcohol to benzaldehyde over MnO_x catalysts is analyzed in the DFT framework
- Oxidation reactivity and selectivity over cluster-sized Mn_4O_8 and Mn_4O_9 catalytic models is compared
- Catalyst poisoning is addressed by investigating the formation of benzoic acid following that of benzaldehyde
- Reaction steps and the related oxidation pathways are collected and analyzed by an original kinetic approach
- Experimental strategies aimed at decreasing catalyst deactivation hence at increasing selectivity are proposed

Benzyl Alcohol to Benzaldehyde Oxidation on MnO_x Clusters: Unraveling Atomistic Features

Laura Gueci[a], Francesco Ferrante[a], Antonio Prestianni[a], Francesco Arena[b,*], Dario Duca[a,*]

[a] *Dipartimento di Fisica e Chimica "Emilio Segrè" - Università degli Studi di Palermo, Viale delle Scienze Ed. 17, I-90128 Palermo, Italy.*
[b] *Dipartimento di Ingegneria - Università degli Studi di Messina, Contrada Di Dio, I-98166 Sant'Agata, Messina, Italy.*

Abstract

The catalytic oxidation of benzyl alcohol with O_2 is a promising option for the production of benzaldehyde, from both environmental and economical viewpoints. In particular, highly dispersed MnO_x systems feature good activity and selectivity in a wide range of temperatures, although deactivation phenomena by over-oxidation and/or poisoning of active sites are generally recorded. On this account, a density functional theory study was performed on cluster-sized catalyst models, namely Mn_4O_8 and over-oxygenated Mn_4O_9 fragments, to predict the reactivity pattern of MnO_x catalysts in the selective aerobic oxidation of benzyl alcohol. Several pathways concur to determine the whole reaction process and all of them were compared to unveil the atomistic details of the alcohol oxidation mechanism. Moreover, assuming that the consecutive formation of benzoic acid affects the activity-stability pattern of the MnO_x based catalyst, also the benzaldehyde oxidation mechanism was computationally addressed. A systematic comparison of the benzyl alcohol and benzaldehyde oxidation mechanisms on the Mn_4O_8 and Mn_4O_9 fragments reveals some experimental strategies to test the reaction mechanisms and design alternative catalytic routes to decrease undesired parasitic reactions leading to catalyst deactivation. The

*Corresponding author
Email addresses: laura.gueci@unipa.it (Laura Gueci), francesco.ferrante@unipa.it (Francesco Ferrante), francesco.arena@unime.it (Francesco Arena), dario.duca@unipa.it (Dario Duca)

matching structural, energetic and kinetic data are published in the Data in Brief journal [1].

Keywords: MnO_x based catalysts, oxidative dehydrogenation, catalyst deactivation, reaction mechanisms, DFT

1. Introduction

The selective oxidation of alcohols to the corresponding carbonyl compounds is an important class of industrial reactions for the production of fine chemicals. In particular, many studies have been devoted to the selective oxidation of benzyl alcohol to benzaldehyde, because of extensive uses of the latter in cosmetics, perfumery, dyestuff and pharmaceutical industries, as the second most important aromatic molecule after vanillin [2–4].

Various oxidizing reagents, such as permanganate and dichromate, are currently employed for the benzaldehyde manufacture processes, although high cost and co-generation of toxic wastes raise severe environmental and economical concerns [5].

Accordingly, Green Chemistry guidelines recommend the heterogeneous catalytic oxidation of benzyl alcohol with oxygen as the most advantageous option for the benzaldehyde manufacture [6]. In this respect, although supported noble-metal catalysts (e.g. Au, Pt, Pd) exhibit good performance under mild reaction conditions [7–15], high costs and deactivation phenomena, due to over-oxidation and/or fouling of active sites, are severe drawbacks for their industrial exploitation [16, 17].

On the other hand, recent literature data on transition metal-oxide catalysts document high activity and selectivity of bare and promoted MnO_x systems in the selective aerobic oxidation of benzyl alcohol to benzaldehyde in a wide range of temperature [18–25]. However, activity loss and the need of regeneration-rejuvenation procedures are generally reported also for such catalysts [6, 26–31]. The latter even shows deactivation phenomena related to the over-oxidation of benzyl alcohol to benzoic acid [32] but the intimate aspects

concerning both the formation of benzoic acid and its role in poisoning the catalyst still deserve investigation. Recent synergistic approaches involving experimental investigations and quantum chemistry calculations, mostly based on Density Functional Theory (DFT), showed to be important in highlighting the fundamental aspects of catalytic reactions enabling the development of effective catalysts and processes [33].

In particular, catalysis performed by clusters involving precise numbers of atoms is a new research area in which the experimental-computational strategy has shown very promising perspectives [33–39]. In fact, the multifaceted panorama of the cluster structures and properties was investigated to design new catalysts whose characteristics could be tuned either changing the elemental nature, sizes and shapes of the clusters or dispersing them on supports having peculiarly addressed features [40–46].

This paper presents a systematic computational study, in the frame of the DFT paradigm, aimed at shedding light on the catalytic mechanisms, even including catalyst deactivation phenomena, which occur in the selective aerobic oxidation of benzyl alcohol to benzaldehyde on MnO_x cluster-sized catalysts [32, 47]. In particular, the role of possible over-oxidizing species, which could potentially lead to the formation of benzoic acid, is investigated. Namely, the role of the oxygen species produced on (or displaced from the bulk to) the catalyst surface, of the O_2 (coming from the gas phase) and of the water molecules (formed during the reaction) was taken into consideration and analyzed. This was done in the hypothesis that benzoic acid or other oxidized intermediates could play a role in the deactivation of the catalyst [32, 47]. The identification of these surface intermediates and especially of the paths determining their genesis could indeed suggest some corrections to be made into the process in order to improve the selectivity to benzaldehyde.

2. Computational Details

The Gaussian 09 package [48] was employed for all the calculations. These were performed in the DFT framework by using the M06-L exchange-correlation functional [49], which showed to be valid in treating inorganic compounds that involve transition metals also when dispersion interactions were relevant. Its reliability for the calculation of barrier heights is demonstrated in previous works for a large number of chemical reactions [50–52] and its accuracy can be quantified by an averaged mean unsigned error of ca. 10 kJ mol^{-1}. The Stuttgart '97 Relativistic Small Core effective potential along with its valence double zeta basis set [53, 54] was used for the Mn atoms whereas the cc-pvDZ basis set was employed for lighter elements. Minima and transition states related to the reaction mechanisms, thoroughly discussed in terms of vibrational zero-point (ZPVE) corrected energies, were characterized by inspection of the harmonic vibrational frequencies. Interaction energies, namely adsorption (ΔE_{ads}) and desorption (ΔE_{des}) energies, were evaluated as the difference between the energy of the adsorbed system and the energies of its constituents. For the interaction energies, basis set superposition error (BSSE) estimated by means of counterpoise procedure [55] is reported. In case of desorption steps, the associated Gibbs free energy (ΔG_{des}) is also given, to get an idea of the expectedly significant role of entropy changes in these event. A kinetic analysis of the catalytic processes was performed following an original approach derived by the classic one of Christiansen [56] and detailed in the Data in Brief (DiB) journal [1]. This method was applied, using ZPVE corrected energies, to compare both the different pathways determining the single reaction mechanisms and the latter ones among themselves [57]. The mutual influence between the various mechanisms studied was conversely not taken into consideration because unimportant with respect of the following discussion and conclusions.

3. Results and discussion

3.1. Catalytic fragments and starting benzyl alcohol adsorption modes

Previous mechanistic results reported by Gueci et al. [32] are summarized in the catalytic cycle of Figure 1. This, in particular, shows the catalytic benzaldehyde oxidation mechanism already proposed after having examined all the possible ways of interaction of the considered molecular substrates with all the plausible adsorption sites present in the different catalytic fragments (Mn_4O_7, Mn_4O_8, Mn_4O_9) involved [32]. The catalytic cycle presents a starting Mn_4O_8 catalytic model cluster — representative of the Mn(IV) sites characterizing the cluster-sized MnO_x fragments present on the surface of real catalysts [6] — that, undergoing transient structural modifications, rules benzyl alcohol oxidation to benzaldehyde, following a complex reaction mechanism. Two benzyl alcohol molecules are transformed into two benzaldehyde and two H_2O molecules, in aerobic conditions.

[Figure 1 about here.]

The Gibbs free energy difference for this process was calculated to be -181.4 kJ mol^{-1}. It has to be noticed that, in order to close the catalytic cycle hence to restore the pristine catalyst, gas-phase O_2 is involved and one Mn_4O_9 fragment is produced along the process. Notably, these fragments may originate either by adsorption of O_2 (from the gas phase) on the pre-reduced cluster (i.e. Mn_4O_7) or by bulk O-atoms diffusion to the surface and/or by surface diffusion of the latter (i.e. spillover).

In fact, several studies performed on MnO_x catalysts actually revealed a certain degree of mobility of surface oxygen species [25, 58–60]. In support of this hypothesis, Oxygen Temperature Programmed Desorption (O2-TPD) analysis performed both on pristine and promoted MnO_x catalysts showed patterns characterized by overwhelming exposures of Mn(IV) active sites [6, 32].

To probe the effects of this phenomenon into the title reaction, hence to investigate the catalytic behavior of a locally over-oxygenated cluster showing a

supposed Mars–van Krevelen (MvK) like mechanism [61], another Mn_4O_9 fragment, aside the complementary one [62] already considered in the second step of the cycle of Figure 1, was additionally taken into consideration in this study. Its optimized geometry, with the most stable spin multiplicity characterizing the same fragment ($2S+1 = 11$), is reported in Figure 2, where the atom labels that will be used in the following are also shown in the left panel [63]. In the right, conversely, an alternative view allows one to distinguish two catalyst halves, arbitrarily labeled top (t) and down (d), with respect to the plane crossing the manganese atoms.

[Figure 2 about here.]

Benzyl alcohol adsorption on the Mn_4O_9 fragment, provided that it actually involves the Mn(D) atom bearing the extra oxygen, may occur either on the side where the O1 and O3 sites are facing upward or on the other side, leading to $Mn(D)_t$ and $Mn(D)_d$ adducts, respectively (see Figure 3). In both cases the benzyl alcohol molecule interacts with the catalyst by its oxygen atom, moreover, in the $Mn(D)_d$ adsorption geometry an interaction between the phenyl fragment and the Mn(A) site is also observed. According to these findings, the $Mn(D)_d$ adsorption system looks to be more stable than the $Mn(D)_t$ one, being the corresponding interaction energies -165.4 kJ mol^{-1} (BSSE= 19.4 kJ mol^{-1}) and -135.5 kJ mol^{-1} (BSSE= 28.1 kJ mol^{-1}), respectively.

[Figure 3 about here.]

The geometrical characteristics and the structural parameters for the two adsorption modes are summarized in Table 1.

[Table 1 about here.]

The main differences essentially rely in the ability of the organic molecule to approach the manganese site, for the most part concerning the interaction distance of the Mn(D) site with the oxygen atom and the aromatic ring of benzyl

alcohol, Mn(D)−O and Mn(D)−C_6H_5, respectively, and the consequent variation of the dihedral angle Θ(O-C-C-C), involving the interacting oxygen and the unsaturated plus a couple of aromatic carbon atoms of the reacting catalytic substrate. The parameter values in Table 1 indicate that the stabilization of the system originates from a stronger interaction of the cluster with the aromatic ring.

[Figure 4 about here.]

It has also to be mentioned that the benzyl alcohol adsorption increased the system spin multiplicity from 11 to 13, irrespective of the considered geometry. The investigated mechanism reported throughout essentially occurs on the $2S+1 = 13$ spin multiplicity surface.

In fact, decreasing/increasing of spin multiplicity, occurring as a result of spin coupling/uncoupling, was found along the reaction path, commonly for species where hydrogen atoms are transferred from the adsorbate to the cluster. The spin multiplicity of the species are always reported along with energetic informations in the corresponding figures. In all cases, an average spin contamination of ca. 2% was found, with maximum values of 6.3%, 2.9% and 3.3%, among the species with $2S + 1 = 11$, 13 and 15 in the order.

In the next section the selective oxidation mechanisms of benzyl alcohol to benzaldehyde on the Mn_4O_9 cluster are detailed. The mechanisms will be labeled as the adsorption geometries from which they start, *i.e.* $Mn(D)_d$ and $Mn(D)_t$. The mechanistic findings, of course, have to be related with the ones already obtained in the oxidation of the second benzyl alcohol molecule ($\Delta E_{ads} = -190.0$ kJ mol^{-1}, BSSE= 22.5 kJ mol^{-1}, $2S + 1 = 11$) on a Mn_4O_9 fragment, involved in the cycle of Figure 1.

3.2. Benzyl alcohol oxidation to benzaldehyde

The first step in the $Mn(D)_d$ reaction pathway is the hydroxyl hydrogen transfer to the Od′ site, overcoming an energy barrier of 69.8 kJ mol^{-1} (Figure 4). From this point, the reaction can proceed following three different ways: i)

the second hydrogen atom is transferred to the O3 site with an energy barrier of 96.3 kJ mol^{-1} and a $(H+H)/Mn_4O_9-C_6H_5$-CHO system, in a spin multiplicity state of 15, is formed, ii) the adsorbed molecule rotates so that one hydrogen of the CH_2 moiety points towards the Od$''$ site, requiring 4.7 kJ mol^{-1} of energy, iii) the hydrogen bonded to the Mn_4O_9 cluster flips downward.

In the first case an over-hydrogenated catalyst with an extra oxygen atom would be obtained after benzaldehyde desorption. The hydrogen hopping in the direction of one of the extra oxygen on the Mn_4O_9 fragment would lead to a water molecule, whose desorption could restore the Mn_4O_8 fragment; however this resulted energetically almost impossible. On the contrary, the involvement of an adsorbed O_2 from the gas phase (even after the desorption of water) would lead to an unlikely hyper-oxygenated Mn_4O_{10} fragment. Given this and realizing that the energy barriers of the other two reaction paths, having common origin, are much lower, this reaction way was not further investigated.

The second reaction path continues with the CH_2 hydrogen being transferred to the Od$'$ site, overcoming a high energy barrier of 150.7 kJ mol^{-1}. The so formed system exhibit a hydrogen bond between the carbonyl oxygen of benzaldehyde and the closest H of a kind of hydrogen peroxide species adsorbed on the Mn(D) site.

Also in this case the same considerations apply as regards the elimination of water through the adsorption of one O_2 molecule while it is still difficult to restore the Mn_4O_8 fragment through the formation of H_2O after the eventual transformation of the H_2O_2-like moiety.

The third reaction path (following the green arrows in Figure 4), with an energy barrier of 15.8 kJ mol^{-1}, might be the favored one among the three investigated. Following this step, once the hydrogen bonded to the vicinal Od$'$ oxygen atom of the the fragment catalysts points downward, one hydrogen of the $-CH_2$ moiety could be subjected to intramolecular migration to the oxygen atom or, alternatively, could be transferred either to Od$'$ or Od$''$. Since the intramolecular shift shows an energy barrier value equal to 181.4 kJ mol^{-1}, the evolution of the mechanism through this pathway was considered as improbable.

The rotation of the dehydrogenated alcohol so that the hydrogen of the CH_2 moiety points towards Od$''$ leads to a species that has a slightly higher energy (4.2 kJ mol^{-1}) but the following step, *i.e.* the hydrogen transfer to the catalyst, needs the overcoming of a prohibitive energy barrier, that is 182.1 kJ mol^{-1}. It is interesting to note that also in this case a species resembling a hydrogen peroxide molecule has formed.

The last reaction path considered involves 40.6 kJ mol^{-1} for the rotation of the dehydrogenated alcohol, causing the CH_2 hydrogen pointing towards the Od$'$ site. This is a pretty high value for a torsional energy, probably originated because the favorable interaction between the phenyl group and the catalyst fragment is missing in the final structure. When the second hydrogen atom of the alcohol is transferred to the already protonated Od$'$ site with an energy barrier of 78.2 kJ mol^{-1}, the system $(C_6H_5{-}CHO + H_2O)/Mn_4O_8$ is formed. The latter then evolves in the three isolated components, needing an energy of 79.7 kJ mol^{-1} (BSSE= 44.6 kJ mol^{-1}), being the ΔG_{des} value equal to 12.1 kJ mol^{-1}.

Figure 5 details the reaction mechanism occurring on the Mn(D)$_t$ site. As found in case of the Mn(D)$_d$ adsorption geometry discussed above, it begins with the hydroxyl hydrogen transfer to the Od$'$ site, overcoming, this time, an energy barrier of 91.1 kJ mol^{-1}. The subsequent hydrogen loss occurs in favor of the closest O2, with an energy barrier of 22.9 kJ mol^{-1}. Thus, a system consisting of one benzaldehyde molecule adsorbed on a hydrogenated Mn_4O_9 catalytic fragment, in a spin state of 15, is obtained. Although this fragment is easily formed, the distance of hydrogen atoms hinders an easy formation of one water molecule (to be desorbed). Given this and considering that the only alternative mechanism would involve an O_2 molecule producing water and the already discarded, because unlikely, hyper-oxygenated Mn_4O_{10} fragment, further investigation neither have been carried out on the product of this parasitic mechanism nor alternative mechanism on the Mn(D)$_t$ site have been taken into consideration. As a consequence, the already selected green pathway of the Mn(D)$_d$ site has been identified as the one occurring in the benzyl alcohol

oxidation on the Mn_4O_9 cluster considered here.

[Figure 5 about here.]

3.3. Energetics of the reaction occurring on Mn_4O_8 and Mn_4O_9 clusters

It is worth to compare the proposed mechanism with that previously suggested for the same reaction occurring on a model Mn_4O_8 cluster, which could be assumed as the precursor of the Mn_4O_9 one. For this purpose, an analysis based on the Christiansen's method of the intermediate quasi-stationary concentrations, was employed [56]. The matrix approach, which lies at its base, allows one to determine the rate of a reaction from the knowledge of the probability of occurrence (per unit of time) of the single elementary steps that compose the same reaction. These probabilities can be related to the theoretically calculated energy barriers, using the Eyring's equation [64–67].

Details on the simplified form of the Christiansen's method here used, hereafter identified as *SCM*, are given elsewhere [1]. It should be here underlined however that by means of *SCM* it is possible to compare either the different probability of occurrence characterizing the pathways which contribute to determining a given reaction stoichiometry or also different reactions in order to establish the most probable among these.

Referring to the title reaction, it can be said that either TOF evaluated at 343 K or the activation energy of the whole reaction, evaluated by an Arrhenius plot in the temperature range in-between 333 and 363 K, both calculated by the M1 *SCM* reaction rates (see Table 2), are in well agreement with the corresponding descriptors experimentally obtained at the same temperatures for the real MnO_2 catalysts [1, 6, 47]. In particular, either the experimental or the calculated TOF/s^{-1} values resulted equal to $4 \cdot 10^{-4}$. Moreover, using *SCM*, and setting the temperature at 343 K it is possible to observe that the mechanism marked by green arrows is the most heuristic, among those ending with the formation of benzaldehyde in Figure 4, due to the intrinsic difficulty to interconvert the H_2O_2-like moieties into the H_2O ones.

[Table 2 about here.]

Conversely, as demonstrated by the *SCM* pathway rate values, reported in Table 2, the mechanism leading to the formation of benzaldehyde from benzyl alcohol on the Mn_4O_8 fragment of Figure 1 is apparently more *facile* than that which occurs on the Mn_4O_9 fragment shown in the same figure. The latter should occur also more laboriously than the ones taking place on the Mn_4O_9 fragment of Figure 4. *SCM* however suggests that the Mn_4O_9 fragment of Figure 1 is, in fact, more active than the Mn_4O_8 one up to the aldehyde desorption step [1]. Conversely, the relative desorption energy, ΔE_{des}, calculated for the two processes occurring on Mn_4O_9 and Mn_4O_8, 231.7 and 110.8 kJ mol^{-1} in the order, proved that the desorption step is more difficult in the former than in the latter and overall suggests that the aldehyde formed on Mn_4O_9 could remain stuck on this fragment. Just to make a qualitative comparison, the probability per unit of time of benzaldehyde desorption at 343 K from the Mn_4O_8 fragment compared to that which occurs from the Mn_4O_9 fragment is ca. $3 \cdot 10^{18}$ times larger. This SCM result is close in agreement with experimental evidences already suggesting that the reaction kinetics were controlled by adsorption–desorption processes [47].

In any case, the process of Figure 4 should be irrelevant with respect to those of Figure 1 with regard to the selective production of benzaldehyde from benzyl alcohol. While, that of Figure 5 should occur as a parallel/parasitic pathway more easily (M5 pathway mechanism of Table 2) but leaving a di-hydrogenated Mn_4O_9 fragment difficult to be reconverted in the starting Mn_4O_8 one [1].

Considering that the Mn_4O_9 fragments could originate by intra-structural migration of reticular oxygens (or by surface spillover as in the case of MnO_x dispersed in other metal-oxides, e.g. $MnCeO_x$ catalysts [68, 69]), it can be concluded that strong sticking of benzaldehyde on MnO_x fragments could also occur in the presence of MvK mechanisms. Due to the oxygen diffusion, a given MvK mechanism has to be associated with an occurrence probability, function of the temperature, which must be taken into account. Therefore, it

is possible to infer that at lower temperatures the Mn_4O_8 cluster should be the one mainly involved in the beginning reaction mechanism. As the temperature rises, conversely, the catalytic system, reaching the energy at which the oxygen diffusion process is triggered, should evolve (also in the initial phases of the reaction) through the steps occurring on the Mn_4O_9 fragment of Figure 1, with a relative change in the benzaldehyde production rate caused by the higher benzaldehyde desorption energy involved on these over-oxygenated fragment.

3.4. Benzoic acid formation

Previous mechanistic studies indicated that the incipient formation of benzoic acid is at the origin of the progressive activity loss of MnO_x catalysts during the selective benzyl alcohol oxidation to benzaldehyde [47]. This prompted us to focus on the consecutive oxidation of benzaldehyde on the Mn_4O_8 cluster to get insights into the factors triggering the over-oxidation process leading to the formation of benzoic acid.

It is known that the hydrated form of benzaldehyde, namely gem-diol, can undergo further oxidation. Taking into consideration this and the findings of the preceding section, the final arrangement of benzaldehyde and water very strongly co-adsorbed on the Mn(A) site of the Mn_4O_8 cluster, produced in the second benzyl alcohol oxidation step [32] of Figure 1, was identified as the probable starting point for the benzoic acid formation, eventually through the intermediate evolution of formed gem-diol.

Figure 6 shows the proposed mechanism in details. The first step involves the shift of one hydrogen atom of the water molecule to the catalytic fragment, with an energy barrier of 63.4 kJ mol^{-1}, and then the successive migration of the OH group on the carbonyl carbon of benzaldehyde, overcoming an energy barrier of 74.5 kJ mol^{-1}. At this point, a comb of different alternative possibilities could be identified:

a) the hydrogen atom bonded to the carbonyl is transferred to the O2 site already involved in the previous step. Although benzoic acid formation

occurs, with an energy barrier of 118.9 kJ mol^{-1}, the residual hydrogenated cluster would suffer a strong distortion, hardly admissible in a real catalytic fragment;

b) after an internal rearrangement for which ca. 22 kJ mol^{-1} are required, the hydrogen atom bonded to the carbonyl is transferred either to the second O2 oxygen or to the O3 site of the C_{2h} Mn_4O_8 cluster, overcoming energy barriers of 45.3 kJ mol^{-1} and 48.8 kJ mol^{-1}, respectively. The formation of a benzoic acid molecule leaves a $(H+H)/Mn_4O_8$ system that can restore the pristine Mn_4O_8 fragment by reaction with gas phase O_2, similarly to what happens in the alcohol to aldehyde oxidation mechanism (see Figure 1). The acid ΔE_{des} was calculated to be 181.8 kJ mol^{-1} (BSSE= 38.5 kJ mol^{-1}), being $\Delta G_{des} = 130.7$ kJ mol^{-1}. This high value is in agreement with the experimental results, showing trace amounts of acid adsorbed on the catalyst [47];

c) The hydrogen atom on the catalyst rotates freely, from below to above the plane, then, overcoming an energy barrier of 40.4 kJ mol^{-1}, it migrates to the carbonyl oxygen of the oxydrilated benzaldehyde, ϕC(OH)HO, with the formation of a η^2 gem-diol/manganese system, *i.e.* with both oxygen atoms of the gem-diol bonded to the same manganese atom and the hydroxyl hydrogen atoms on the same side. The latter afterwards evolves spontaneously into a more stable gem-diol, with a single oxygen atom bonded to manganese and the hydroxyl hydrogen atoms placed on opposite sides. This species yields the hydrogen atom bonded to quaternary carbon to the catalyst, with a barrier of 111.7 kJ mol^{-1}, and the protonated carboxylic acid thus formed subsequently releases the proton in a non-activated process. Benzoic acid and the $(H + H)/Mn_4O_8$ system are eventually obtained.

[Figure 6 about here.]

Although the transformation of benzaldehyde into benzoic acid could be

induced by the gem-diol intermediate, it can be assumed that the gem-diol does not evolve into acid since the process is limited by the above energy barrier (111.7 kJ mol^{-1}). Therefore, benzaldehyde oxidizes directly into acid after path b), in particular, following the branch in which the largest energy barrier, aside the one originating the ϕC(OH)HO formation (common to all the paths), is ca. 49 kJ mol^{-1}. This inference is confirmed applying *SCM* to the different paths (see Table 2), ending in the same stoichiometric process reported in Figure 6. In particular, *SCM* shows that the chosen mechanism is characterized by a whole reaction rate which is, at 343 K, ca. 40 times larger than that of the other one and this mainly depends on the higher desorption energy characterizing the mechanism of the latter. Indeed, *SCM* also shows that the more numerous surface steps of the gem-diol pathway are sometimes less favored with respect to those of the other two pathways but that the production of benzoic acid *via* the gem-diol intermediate is on the whole comparable to that of the faster of the two. This because the whole processes should be mainly ruled by the acid desorption energies.

Finally, using once again *SCM* to juxtapose the two reactions involved in the whole oxidation mechanisms, namely alcohol $\longrightarrow$ aldehyde and aldehyde $\longrightarrow$ acid processes, it can be observed, referring to the corresponding fastest pathways, that the former, when the same concentrations of initial reactant surface species are considered, would be favored. In fact, the ratio of the corresponding reaction rate values, mostly determined by the desorption steps of the involved products [1], is equal to ca. $7 \cdot 10^{10}$, at 343 K (see Table 2). These findings that underline that the rate of the surface steps of the different oxidation processes are not particularly influent on the whole reaction rates, would seem to confirm the benzoic acid poisoning role [47] in the selective benzyl alcohol oxidation to aldehyde on MnO_x based catalysts.

3.5. How to use the computational findings in practice

According to the above findings, the co-presence of benzaldehyde and water on the catalyst is the potential cause of benzoic acid formation, leading to

catalyst deactivation. In fact, the adsorbed water plays a crucial role in the reduction of selectivity to benzaldehyde, due to the transfer of one hydroxyl group from a water to a benzaldehyde molecule. Therefore, it is admissible to hypothesize that dehydrating the system during the reaction or, as a preventive strategy, avoiding the formation of water on the cluster, in the presence of benzaldehyde, could represent a way to limit the acidic by-product formation.

Water formation occurs in two stages of the presented benzyl alcohol to benzaldehyde oxidation mechanism: i) when the O_2 adsorbs on the di-hydrogenated catalytic fragment, $(H+H)/Mn_4O_8$, transforming it into the intermediate Mn_4O_9 species and ii) when one alcohol molecule is oxidized by the different Mn_4O_9 fragments (see Figures 1 and 4).

Formation of water hence would seem to be related either to the presence of gas phase oxygen or to the occurrence of MvK mechanisms. Nevertheless, for the benzyl alcohol to benzaldehyde oxidation on the Mn_4O_8 cluster (first step of Figure 1) not oxygen intervention would seem to be required, being O_2 conversely necessary, as underlined above, just to eliminate the hydrogen atoms on the same Mn_4O_8 fragment after the first alcohol molecule oxidation.

Hence, either to decrease benzoic acid formation or, at least, to test the network of mechanisms suggested here, it could be possible to carry out the selective oxidation of benzyl alcohol just on the pristine (Mn_4O_8) fragments. For this, it could be appropriate to lower the temperature, hence to reduce either intra-structural oxygen or spillover surface migrations, and to co-feed the system, in sequence and cyclically, by benzyl alcohol, O_2 and finally CO (see Table 2). The MnO_x based catalysts are indeed also active in the oxidation of carbon monoxide [68, 69]. This sequential procedure starting with ϕCH_2OH and characterized by the following stoichiometric processes:

$$\phi CH_2OH + Mn_4O_8 \longrightarrow (H + H)/Mn_4O_8 + \phi CHO \tag{1}$$

$$(H + H)/Mn_4O_8 + O_2 \longrightarrow Mn_4O_9 + H_2O \tag{2}$$

$$Mn_4O_9 + CO \longrightarrow Mn_4O_8 + CO_2 \tag{3}$$

could help, as shown by the *SCM* analysis on steps 2 and 3, see M2 and M9 in Table 2, (by step 2) to eliminate, forming H_2O, the hydrogen present on the stoichiometric (Mn_4O_8) fragments and (by step 3) to reduce, forming CO_2, the over-oxygenated (Mn_4O_9) derivatives, shaped in the preceding step, before another alcohol molecule would undergo oxidation again on Mn_4O_8. In this way the apparent catalytic cycle summarized below:

$$\phi CH_2OH + CO + O_2 \xrightarrow{Mn_4O_8} \phi CHO + H_2O + CO_2$$

would be closed.

It can finally be observed that this reaction design would also limit parasitic poisoning processes on Mn_4O_9 fragments, potentially able to deactivate the Mn_4O_8 catalyst. In particular, the oxidation processes of the benzyl alcohol occurring on Mn_4O_9, such as the one, represented in Figure 1, that is characterized by the almost irreversible sticking of benzaldehyde able to initiate, in presence of water, the benzoic acid formation or the other, represented in Figure 5, which is indeed the fastest oxidation process (see M5 rate value in Table 2) that however leaves the Mn_4O_9 fragment in a di-hydrogenated form, from which, as already stated, it is difficult to recover the initial catalytic conditions.

4. Conclusions

A DFT analysis of the benzyl alcohol oxidation on MnO_x clusters has been performed. In addition to one stoichiometric (Mn_4O_8) cluster, over-oxygenated (Mn_4O_9) derivatives, originated by both O_2 and/or intra-structural and/or surface spillover oxygenation (MvK mechanism) were considered. Having explored a wide panorama of possibilities, all the reactions paths have been compared and it was thus possible to select the most likely mechanism for the benzyl alcohol oxidation to benzaldehyde. The parallel benzaldehyde to benzoic acid oxidation has been also addressed in order to find a way to increase the selectivity of the MnO_x based catalysts and to state its, already hypothesized, poisoning role. The atomistic understanding of the mechanism concerning the benzoic acid formation has allowed us to outline some strategies for experimental work, referred

to the title reaction. These are addressed: *i*) to validate the already proposed experimental mechanism; *ii*) to test the here proposed reaction network; *iii*) to improve, if the proposed mechanism shows eventually to be valid, the selectivity of the benzyl alcohol oxidation process over MnO_x derived catalysts.

References

[1] L. Gueci, F. Ferrante, A. Prestianni, F. Arena, D. Duca, Structural, energetic and kinetic database of catalytic reactions: Benzyl alcohol to benzaldehyde oxidation on MnO_x clusters, Data Brief 000 (0) (2021) 0000–0000. doi:10.1016/j.dib.xxxx.xx.xxx.

[2] F. Brühne, E. Wright, Benzaldehyde, in: B., et al. Elvers (Ed.), Ullmann's Encyclopedia of Industrial Chemistry, Vol. 5, Wiley-VCH, Weinheim, 2011, pp. 224–235.

[3] F. Su, S. C. Mathew, G. Lipner, X. Fu, M. Antonietti, S. Blechert, X. Wang, mpg-C_3N_4-Catalyzed Selective Oxidation of Alcohols Using O_2 and Visible Light, J. Am. Chem. Soc. 132 (46) (2010) 16299–16301. doi:10.1021/ja102866p.

[4] L. Jia, S. Zhang, F. Gu, Y. Ping, X. Guo, Z. Zhong, F. Su, Highly selective gas-phase oxidation of benzyl alcohol to benzaldehyde over silver-containing hexagonal mesoporous silica, Micropor. Mesopor. Mat. 149 (1) (2012) 158–165. doi:https://doi.org/10.1016/j.micromeso.2011.08.009.

[5] J. Liu, X.-P. Wu, S. Zou, Y. Dai, L. Xiao, X.-Q. Gong, J. Fan, Origin of the High Activity of Mesoporous CeO_2 Supported Monomeric VOx for Low-Temperature Gas-Phase Selective Oxidative Dehydrogenation of Benzyl Alcohol: Role As an Electronic "Hole", J. Phys. Chem. C 118 (43) (2014) 24950–24958. doi:10.1021/jp5062094.

[6] F. Arena, B. Gumina, A. F. Lombardo, C. Espro, A. Patti, L. Spadaro, L. Spiccia, Nanostructured MnO_x catalysts in the liquid phase selective

oxidation of benzyl alcohol, with oxygen: Part I. Effects of Ce and Fe addition on structure and reactivity, Appl. Catal. B: Env. 162 (2015) 260–267. doi:https://doi.org/10.1016/j.apcatb.2014.06.054.

[7] X. Wang, H. Kawanami, S. E. Dapurkar, N. S. Venkataramanan, M. Chatterjee, T. Yokoyama, Y. Ikushima, Selective oxidation of alcohols to aldehydes and ketones over TiO_2-supported gold nanoparticles in supercritical carbon dioxide with molecular oxygen, Appl. Catal. A: Gen. 349 (1) (2008) 86–90. doi:https://doi.org/10.1016/j.apcata.2008.07.007.

[8] N. Dimitratos, J. A. Lopez-Sanchez, D. Morgan, A. F. Carley, R. Tiruvalam, C. J. Kiely, D. Bethell, G. J. Hutchings, Solvent-free oxidation of benzyl alcohol using Au–Pd catalysts prepared by sol immobilisation, Phys. Chem. Chem. Phys. 11 (2009) 5142–5153. doi:10.1039/B900151B.

[9] C. Y. Ma, B. J. Dou, J. J. Li, J. Cheng, Q. Hu, Z. P. Hao, S. Z. Qiao, Catalytic oxidation of benzyl alcohol on Au or Au–Pd nanoparticles confined in mesoporous silica, Appl. Catal. B: Env. 92 (1) (2009) 202–208. doi:https://doi.org/10.1016/j.apcatb.2009.07.007.

[10] P. J. Miedziak, Q. He, J. K. Edwards, S. H. Taylor, D. W. Knight, B. Tarbit, C. J. Kiely, G. J. Hutchings, Oxidation of benzyl alcohol using supported gold–palladium nanoparticles, Catal. Today 163 (1) (2011) 47–54. doi:https://doi.org/10.1016/j.cattod.2010.02.051.

[11] M. Boronat, A. Corma, F. Illas, J. Radilla, T. Ródenas, M. J. Sabater, Mechanism of selective alcohol oxidation to aldehydes on gold catalysts: Influence of surface roughness on reactivity, J. Catal. 278 (1) (2011) 50–58. doi:https://doi.org/10.1016/j.jcat.2010.11.013.

[12] A. Savara, I. Rossetti, C. E. Chan-Thaw, L. Prati, A. Villa, Microkinetic modeling of benzyl alcohol oxidation on carbon-supported palladium nanoparticles, ChemCatChem 8 (15) (2016) 2482–2491. doi:10.1002/cctc.201600368.

[13] J. Liu, S. Zou, J. Wu, H. Kobayashi, H. Zhao, J. Fan, Green catalytic oxidation of benzyl alcohol over Pt/ZnO in base-free aqueous medium at room temperature, Chinese J. Catal. 39 (6) (2018) 1081–1089. doi:https://doi.org/10.1016/S1872-2067(18)63022-0.

[14] M. Marelli, A. Jouve, A. Villa, R. Psaro, A. Balerna, L. Prati, C. Evangelisti, Hybrid Au/CuO Nanoparticles: Effect of Structural Features for Selective Benzyl Alcohol Oxidation, J. Phys. Chem. C 123 (5) (2019) 2864–2871. doi:10.1021/acs.jpcc.8b09449.

[15] J. Yang, K. Cao, M. Gong, B. Shan, R. Chen, Atomically decorating of MnO_x on palladium nanoparticles towards selective oxidation of benzyl alcohol with high yield, J. Catal. 386 (2020) 60–69. doi:https://doi.org/10.1016/j.jcat.2020.03.029.

[16] N. Al-Rifai, P. J. Miedziak, M. Morad, M. Sankar, C. Waldron, S. Cattaneo, E. Cao, S. Pattisson, D. Morgan, D. Bethell, G. J. Hutchings, A. Gavriilidis, Deactivation Behavior of Supported Gold Palladium Nanoalloy Catalysts during the Selective Oxidation of Benzyl Alcohol in a Micropacked Bed Reactor, Ind. Eng. Chem. Res. 56 (45) (2017) 12984–12993. doi:10.1021/acs.iecr.7b01159.

[17] S. Guadix-Montero, H. Alshammari, R. Dalebout, E. Nowicka, D. J. Morgan, G. Shaw, Q. He, M. Sankar, Deactivation studies of bimetallic AuPd nanoparticles supported on MgO during selective aerobic oxidation of alcohols, Appl. Catal. A: Gen. 546 (2017) 58–66. doi:https://doi.org/10.1016/j.apcata.2017.07.045.

[18] C. Parmeggiani, F. Cardona, Transition metal based catalysts in the aerobic oxidation of alcohols, Green Chem. 14 (3) (2012) 547–564. doi:10.1039/C2GC16344F.

[19] Y. Chen, H. Zheng, Z. Guo, C. Zhou, C. Wang, A. Borgna, Y. Yang, Pd catalysts supported on $MnCeO_x$ mixed oxides and their catalytic

application in solvent-free aerobic oxidation of benzyl alcohol: Support composition and structure sensitivity, J. Catal. 283 (1) (2011) 34–44. doi:https://doi.org/10.1016/j.jcat.2011.06.021.

[20] Q. Tang, T. Liu, Y. Yang, Role of potassium in the aerobic oxidation of aromatic alcohols over K^+ -protonated Mn/C catalysts, Catal. Commun. 9 (15) (2008) 2570–2573. doi:https://doi.org/10.1016/j.catcom.2008.07.013.

[21] Q. Tang, X. Huang, C. Wu, P. Zhao, Y. Chen, Y. Yang, Structure and catalytic properties of K-doped manganese oxide supported on alumina, J. Mol. Cat. A: Chem. 306 (1) (2009) 48–53. doi:https://doi.org/10.1016/j.molcata.2009.02.020.

[22] T. Sato, T. Komanoya, Selective oxidation of alcohols with molecular oxygen catalyzed by $Ru/MnO_x/CeO_2$ under mild conditions, Catal. Commun. 10 (7) (2009) 1095–1098. doi:https://doi.org/10.1016/j.catcom.2009.01.004.

[23] M. Ilyas, M. Saeed, Synthesis and Characterization of Manganese Oxide and Investigation of its Catalytic Activities for Oxidation of Benzyl Alcohol in Liquid Phase, Int. J. Chem. React. Eng. 9 (1) (2011) A75. doi:https://doi.org/10.1515/1542-6580.2646.

[24] S. Biswas, A. S. Poyraz, Y. Meng, C.-H. Kuo, C. Guild, H. Tripp, S. L. Suib, Ion induced promotion of activity enhancement of mesoporous manganese oxides for aerobic oxidation reactions, Appl. Catal. B: Env. 165 (2015) 731–741. doi:https://doi.org/10.1016/j.apcatb.2014.10.055.

[25] F. Schurz, J. M. Bauchert, T. Merker, T. Schleid, H. Hasse, R. Gläser, Octahedral molecular sieves of the type K-OMS-2 with different particle sizes and morphologies: Impact on the catalytic properties in the aerobic partial oxidation of benzyl alcohol, Appl. Catal. A: Gen. 355 (1) (2009) 42–49. doi:https://doi.org/10.1016/j.apcata.2008.11.014.

[26] J. Fei, L. Sun, C. Zhou, H. Ling, F. Yan, X. Zhong, Y. Lu, J. Shi, J. Huang, Z. Liu, Tuning the Synthesis of Manganese Oxides Nanoparticles for Efficient Oxidation of Benzyl Alcohol, Nanoscale Res. Lett. 12 (1) (2017) 23. doi:10.1186/s11671-016-1777-y.

[27] G. Elmacı, A. S. Ertürk, M. Sevim, Önder Metin, Liquid phase aerobic oxidation of benzyl alcohol by using manganese ferrite supported-manganese oxide nanocomposite catalyst, Catal. Commun. 89 (2017) 56–59. doi:https://doi.org/10.1016/j.catcom.2016.10.027.

[28] G. Elmacı, C. E. Frey, P. Kurz, B. Zümreoğlu-Karan, Water oxidation catalysis by using nano-manganese ferrite supported 1D-(tunnelled), 2D-(layered) and 3D-(spinel) manganese oxides, J. Mater. Chem. A 4 (2016) 8812–8821. doi:10.1039/C6TA00593D.

[29] G. Elmacı, A. S. Ertürk, M. Sevim, Önder Metin, MnO_2 nanowires anchored on mesoporous graphitic carbon nitride (MnO_2@mpg-C_3N_4) as a highly efficient electrocatalyst for the oxygen evolution reaction, Int. J. Hydrogen Energy 44 (33) (2019) 17995–18006. doi:https://doi.org/10.1016/j.ijhydene.2019.05.089.

[30] G. Elmacı, G. Özgenç, P. Kurz, B. Zumreoglu-Karan, Enhanced water oxidation performances of birnessite and magnetic birnessite nanocomposites by transition metal ion doping, Sustainable Energy Fuels 4 (2020) 3157–3166. doi:10.1039/D0SE00301H.

[31] L. Gurrala, A. S. Nagpure, H. R. Gurav, S. Chilukuri, Spinel-Type Mixed Oxides for Stable and Selective Partial Oxidation of Benzyl Alcohol, ChemistrySelect 3 (13) (2018) 3751–3761. doi:10.1002/slct.201800321.

[32] L. Gueci, F. Ferrante, A. Prestianni, R. Di Chio, A. F. Patti, D. Duca, F. Arena, DFT insights into the oxygen-assisted selective oxidation of benzyl alcohol on manganese dioxide catalysts, Inorg. Chim. Acta 511 (2020) 119812. doi:https://doi.org/10.1016/j.ica.2020.119812.

[33] D. K. Pappas, A. Martini, M. Dyballa, K. Kvande, S. Teketel, K. A. Lomachenko, R. Baran, P. Glatzel, B. Arstad, G. Berlier, C. Lamberti, S. Bordiga, U. Olsbye, S. Svelle, P. Beato, E. Borfecchia, The Nuclearity of the Active Site for Methane to Methanol Conversion in Cu-Mordenite: A Quantitative Assessment, J. Am. Chem. Soc. 140 (45) (2018) 15270–15278. doi:10.1021/jacs.8b08071.

[34] F. Ferrante, A. Prestianni, D. Duca, Computational Investigation of Alkynols and Alkyndiols Hydrogenation on a Palladium Cluster, J. Phys. Chem. C 118 (1) (2014) 551–558. doi:10.1021/jp410878j.

[35] A. Prestianni, M. Crespo-Quesada, R. Cortese, F. Ferrante, L. Kiwi-Minsker, D. Duca, Structure Sensitivity of 2-Methyl-3-butyn-2-ol Hydrogenation on Pd: Computational and Experimental Modeling, J. Phys. Chem. C 118 (6) (2014) 3119–3128. doi:10.1021/jp4114859.

[36] R. Cortese, R. Schimmenti, F. Ferrante, A. Prestianni, D. Decarolis, D. Duca, Graph-Based Analysis of Ethylene Glycol Decomposition on a Palladium Cluster, J. Phys. Chem. C 121 (25) (2017) 13606–13616. doi:10.1021/acs.jpcc.7b00850.

[37] R. Schimmenti, R. Cortese, L. Godina, A. Prestianni, F. Ferrante, D. Duca, D. Yu. Murzin, A Combined Theoretical and Experimental Approach for Platinum Catalyzed 1,2-Propanediol Aqueous Phase Reforming, J. Phys. Chem. C 121 (27) (2017) 14636–14648. doi:10.1021/acs.jpcc.7b03716.

[38] H. Yuan, J. Chen, Y. Guo, H. Wang, P. Hu, Insight into the Superior Catalytic Activity of MnO_2 for Low-Content NO Oxidation at Room Temperature, J. Phys. Chem. C 122 (44) (2018) 25365–25373. doi:10.1021/acs.jpcc.8b07330.

[39] G. Elmacı, A. S. Ertürk, M. Sevim, Önder Metin, The syntheses, molecular structure analyses and DFT studies on new benzil monohydrazone based Schiff bases, J. Mol. Struct. 1162 (2018) 37–44. doi:https://doi.org/10.1016/j.molstruc.2018.02.035.

[40] D. Duca, F. Ferrante, G. La Manna, Theoretical Study of Palladium Cluster Structures on Carbonaceous Supports, J. Phys. Chem. C 111 (14) (2007) 5402–5408. doi:10.1021/jp067167k.

[41] V. D'Anna, D. Duca, F. Ferrante, G. La Manna, DFT studies on catalytic properties of isolated and carbon nanotube supported Pd_9 cluster–I: adsorption, fragmentation and diffusion of hydrogen, Phys. Chem. Chem. Phys. 11 (20) (2009) 4077–4083. doi:10.1039/B820707K.

[42] V. D'Anna, D. Duca, F. Ferrante, G. La Manna, DFT studies on catalytic properties of isolated and carbon nanotube supported Pd_9 cluster Part II. Hydro-isomerization of butene isomers, Phys. Chem. Chem. Phys. 12 (6) (2010) 1323–1330. doi:10.1039/B920949M.

[43] A. Prestianni, F. Ferrante, E. M. Sulman, D. Duca, Density Functional Theory Investigation on the Nucleation and Growth of Small Palladium Clusters on a Hyper-Cross-Linked Polystyrene Matrix, J. Phys. Chem. C 118 (36) (2014) 21006–21013. doi:10.1021/jp506320z.

[44] R. Schimmenti, R. Cortese, F. Ferrante, A. Prestianni, D. Duca, Growth of sub-nanometric palladium clusters on boron nitride nanotubes: a DFT study, Phys. Chem. Chem. Phys. 18 (3) (2016) 1750–1757. doi:10.1039/C5CP06625E.

[45] F. Ferrante, A. Prestianni, R. Cortese, R. Schimmenti, D. Duca, Density Functional Theory Investigation on the Nucleation of Homo- and Heteronuclear Metal Clusters on Defective Graphene, J. Phys. Chem. C 120 (22) (2016) 12022–12031. doi:10.1021/acs.jpcc.6b02833.

[46] A. Prestianni, R. Cortese, F. Ferrante, R. Schimmenti, D. Duca, S. Hermans, D. Yu. Murzin, α-D-Glucopyranose Adsorption on a Pd_{30} Cluster Supported on Boron Nitride Nanotube, Top. Catal. 59 (2016) 1178–1184. doi:https://doi.org/10.1007/s11244-016-0638-3.

[47] F. Arena, B. Gumina, C. Cannilla, L. Spadaro, A. Patti, L. Spiccia, Nanostructured MnO_x catalysts in the liquid phase selective oxidation of benzyl alcohol with oxygen: Part II. Reaction mechanism, kinetics and deactivation pattern, Appl. Catal. B: Env. 170-171 (2015) 233–240. doi:https://doi.org/10.1016/j.apcatb.2015.01.040.

[48] M. J. Frisch, G. W. Trucks, H. B. Schlegel, G. E. Scuseria, M. A. Robb, J. R. Cheeseman, G. Scalmani, V. Barone, B. Mennucci, G. A. Petersson, H. Nakatsuji, M. Caricato, X. Li, H. P. Hratchian, A. F. Izmaylov, J. Bloino, G. Zheng, J. L. Sonnenberg, M. Hada, M. Ehara, K. Toyota, R. Fukuda, J. Hasegawa, M. Ishida, T. Nakajima, Y. Honda, O. Kitao, H. Nakai, T. Vreven, J. J. A. Montgomery, J. E. Peralta, F. Ogliaro, M. Bearpark, J. J. Heyd, E. Brothers, K. N. Kudin, V. N. Staroverov, R. Kobayashi, J. Normand, K. Raghavachari, A. Rendell, J. C. Burant, S. S. Iyengar, J. Tomasi, M. Cossi, N. Rega, J. M. Millam, M. Klene, J. E. Knox, J. B. Cross, V. Bakken, C. Adamo, J. Jaramillo, R. Gomperts, R. E. Stratmann, O. Yazyev, A. J. Austin, R. Cammi, C. Pomelli, J. W. Ochterski, R. L. Martin, K. Morokuma, V. G. Zakrzewski, G. A. Voth, P. Salvador, J. J. Dannenberg, S. Dapprich, A. D. Daniels, Ö. Farkas, J. B. Foresman, J. V. Ortiz, J. Cioslowski, D. J. Fox, Gaussian 09 Revision D.01, gaussian Inc. Wallingford CT 2009.

[49] Y. Zhao, D. G. Truhlar, A new local density functional for main-group thermochemistry, transition metal bonding, thermochemical kinetics, and noncovalent interactions, J. Chem. Phys. 125 (19) (2006) 194101. doi:10.1063/1.2370993.

[50] Y. Sun, H. Chen, Performance of Density Functionals for Activation Energies of Zr-Mediated Reactions, J. Chem. Theory Comp. 9 (11) (2013) 4735–4743. doi:10.1021/ct400432x.

[51] Y. Sun, H. Chen, Performance of Density Functionals for Activation En-

ergies of Re-Catalyzed Organic Reactions, J. Chem. Theory Comp. 10 (2) (2014) 579–588. doi:10.1021/ct4010855.

[52] L. Hu, H. Chen, Assessment of DFT Methods for Computing Activation Energies of Mo/W-Mediated Reactions, J. Chem. Theory Comp. 11 (10) (2015) 4601–4614. doi:10.1021/acs.jctc.5b00373.

[53] M. Dolg, U. Wedig, H. Stoll, H. Preuss, Energy-adjusted *ab initio* pseudopotentials for the first row transition elements, J. Chem. Phys. 86 (2) (1987) 866–872. doi:10.1063/1.452288.

[54] J. M. L. Martin, A. Sundermann, Correlation consistent valence basis sets for use with the Stuttgart–Dresden–Bonn relativistic effective core potentials: The atoms Ga–Kr and In–Xe, J. Chem. Phys. 114 (8) (2001) 3408–3420. doi:10.1063/1.1337864.

[55] S. Boys, F. Bernardi, The calculation of small molecular interactions by the differences of separate total energies. Some procedures with reduced errors, Mol. Physics 19 (4) (1970) 553–566. doi:10.1080/00268977000101561.

[56] J. A. Christiansen, The elucidation of reaction mechanisms by the method of intermediates in quasi-stationary concentrations, Adv. Cat. 5 (1953) 311–353. doi:https://doi.org/10.1016/S0360-0564(08)60644-6.

[57] DiB article [1] reports tables and figures concerning the optimized Cartesian coordinates as well as the absolute and the relative energies of significant species (reactants, intermediates, transition states and products) involved in the different heterogeneous reaction pathways that concur to define the title oxidation mechanisms. It also illustrates the development of an original model, derived by the classic Christiansen's method, that employs the above energy values to generate data on the reaction kinetics and on the corresponding population of the different surface species, which are outlined in DiB too. This clearly allows one to discriminate among the properties of the different reaction pathways concurring to define the stoichiometric surface processes as here shown on the basis of just *in silico* evaluation.

[58] V. Santos, M. Pereira, J. Órfão, J. Figueiredo, The role of lattice oxygen on the activity of manganese oxides towards the oxidation of volatile organic compounds, Appl. Catal. B: Env. 99 (1) (2010) 353–363. doi:https://doi.org/10.1016/j.apcatb.2010.07.007.

[59] Y.-G. Yin, W.-Q. Xu, Y.-F. Shen, S. L. Suib, C. L. O'Young, Studies of Oxygen Species in Synthetic Todorokite-like Manganese Oxide Octahedral Molecular Sieves, Chem. Mater. 6 (10) (1994) 1803–1808. doi:10.1021/cm00046a038.

[60] V. D. Makwana, Y.-C. Son, A. R. Howell, S. L. Suib, The Role of Lattice Oxygen in Selective Benzyl Alcohol Oxidation Using OMS-2 Catalyst: A Kinetic and Isotope-Labeling Study, J. Catal. 210 (1) (2002) 46–52. doi:https://doi.org/10.1006/jcat.2002.3680.

[61] C. Doornkamp, V. Ponec, The universal character of the Mars and Van Krevelen mechanism, J. Mol. Cat. A: Chem. 162 (2000) 19–32. doi:https://doi.org/10.1016/S1381-1169(00)00319-8.

[62] Given the C_{2h} symmetry of the Mn_4O_8 fragment, there are just two different Mn centers to be considered for placing the extra O atom on the cluster.

[63] When the Mn_4O_8 cluster was considered in the oxidation process [32], one Mn(A) center was modified during the reaction generating a topologically different site that was therefore labeled as Mn(C). In this work it is a site Mn(B) which, due to the presence of the two oxygens bonded, determines asymmetry both on the Mn(A) and on the Mn(B) sites. Considering the present one as the extension of the aforementioned work, it was preferred, for homogeneity, to indicate the over-oxygenated Mn(B) site as Mn(D) and not as Mn(C) while, for the sake of simplicity, no label variation was specified for the residual Mn(B) site. The not involved Mn(A) center and oxygen atoms linked to Mn(D) are not labeled because not significant in the discussion.

[64] D. Duca, L. Botár, T. Vidóczy, Monte Carlo Simulation of Ethylene Hydrogenation on Pt Catalysts, J. Catal. 162 (2) (1996) 260–267. doi:https://doi.org/10.1006/jcat.1996.0283.

[65] D. Duca, P. Baranyai, T. Vidóczy, Monte-carlo model for the hydrogenation of alkenes on metal catalyst, J. Comput. Chem. 19 (4) (1998) 396–403. doi:https://doi.org/10.1002/(SICI)1096-987X(199803)19:4<396::AID-JCC2>3.0.CO;2-N.

[66] D. Duca, Zs. Varga, G. La Manna, T. Vidóczy, Hydrogenation of acetylene–ethylene mixtures on Pd catalysts: study of the surface mechanism by computational approaches. Metal dispersion and catalytic activity, Theor. Chem. Acc. 104 (3) (2000) 302–311. doi:10.1007/s002140000123.

[67] S. Kozuch, S. Shaik, A combined kinetic-quantum mechanical model for assessment of catalytic cycles: Application to Cross-Coupling and Heck reactions, J. Am. Chem. Soc. 128 (2005) 3355–3365. doi:https://doi.org/10.1021/ja0559146.

[68] F. Arena, R. Di Chio, C. Espro, A. Palella, L. Spadaro, A definitive assessment of the CO oxidation pattern of a nanocomposite $MnCeO_x$ catalyst, React. Chem. Eng. 3 (2018) 293–300. doi:10.1039/C8RE00026C.

[69] F. Arena, R. Di Chio, C. Espro, B. Fazio, A. Palella, L. Spadaro, A New Class of $MnCeO_x$ Materials for the Catalytic Gas Exhausts Emission Control: A Study of the CO Model Compound Oxidation, Topics in Catalysis 62 (1) (2019) 259–265. doi:10.1007/s11244-018-1113-0.

List of Figures

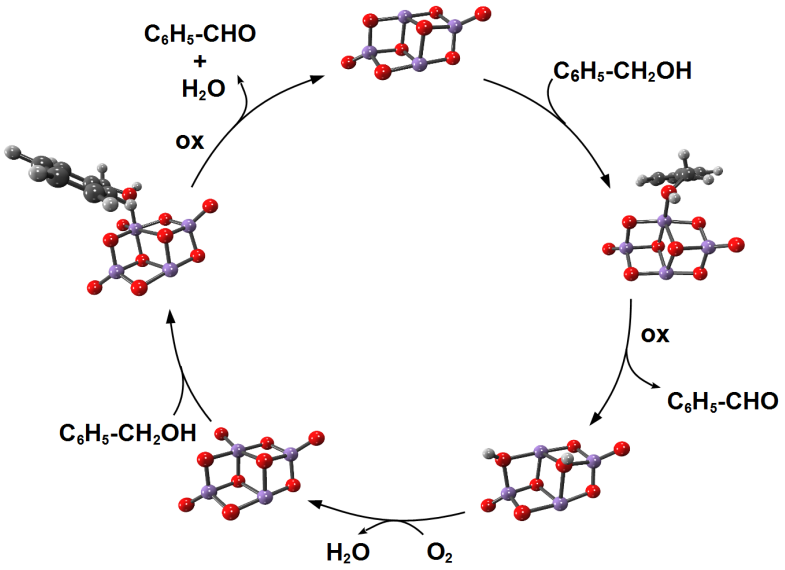

Figure 1: Catalytic cycle on the Mn_4O_8 cluster. At first, one C_6H_5-CH_2OH molecule is adsorbed on the Mn_4O_8 catalytic fragment and oxidized to benzaldehyde; following the benzaldehyde desorption a residual di-hydrogenated catalyst is shaped and transformed into an intermediate Mn_4O_9 cluster by the involvement of molecular O_2. Finally, the intermediate catalytic fragment above rules the oxidation of a second benzyl alcohol molecule and returns to the starting Mn_4O_8 form, thus closing the catalytic cycle. Two H_2O molecules are clearly formed along with the occurrence of the process.

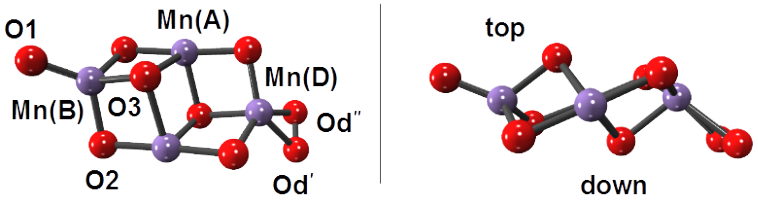

Figure 2: Two perspectives of the Mn_4O_9 fragment, optimized in the spin state $2S + 1 = 11$. On the left, the labels assigned to non-equivalent atoms are shown. On the right, the catalytic fragment is ideally divided by a plane passing through the four manganese atoms in an upper region (top), in which both the O1 and O3 oxygens are facing upward, and in a lower one (down). Notice that Mn(A) and Mn(B) were the indexing used for couples of the same sites on a Mn_4O_8 fragment [32] of C_{2h} symmetry (see Figure 1), from which the Mn_4O_9 fragment (approximately C_s) was originated.

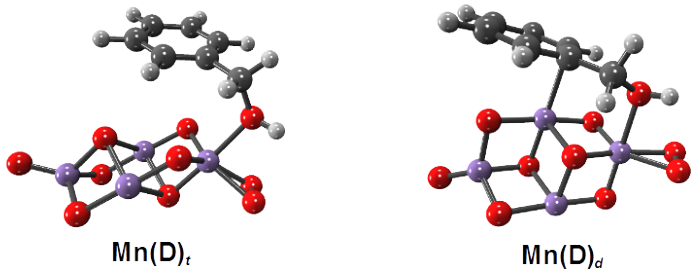

Figure 3: $Mn(D)_t$ and $Mn(D)_d$ adsorption modes of the benzyl alcohol molecule on the Mn_4O_9 cluster.

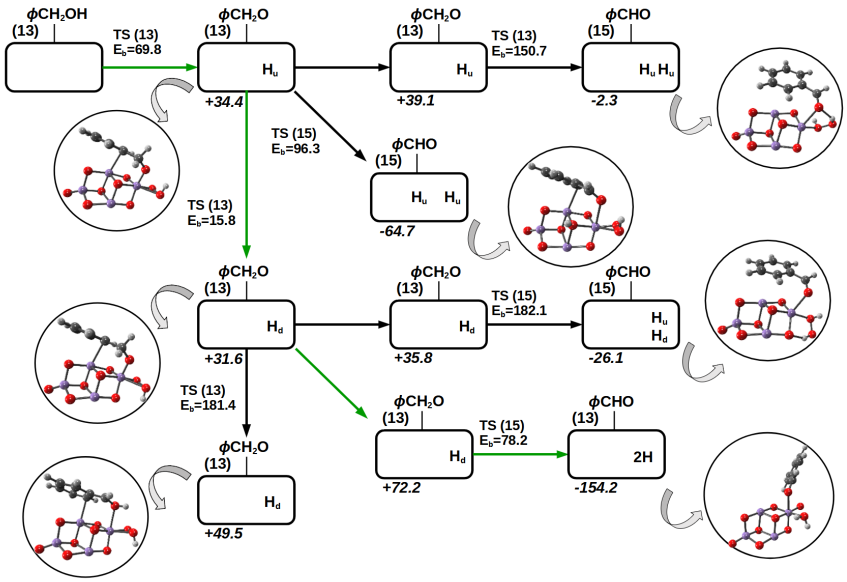

Figure 4: Possible $Mn(D)_d$ reaction mechanisms, which consist in the oxidation of a benzyl alcohol (ϕCH_2OH) molecule on the over-oxygenated Mn_4O_9 cluster. All the minimum species involved are schematically reported and for the species of particular interest a visual representation is given. The rectangle represents the starting Mn_4O_9 cluster. Rectangle with one H_u or H_d indicates a singly hydrogenated Mn_4O_9 fragment, indicating the subscripts "u" and "d" that the hydrogen atom points upward or downward. Rectangles with two hydrogens straightforwardly represent di-hydrogenated fragments and the hydrogen specification inside intends, instead, to distinguish among the different local topologies (see the corresponding structures). ϕCH_2O represents dehydrogenated benzyl alcohol while ϕCHO benzaldehyde. Energy barriers corresponding to the transition states and energies of all minima with respect to the species from which the mechanism begins (taken as reference) are also indicated. Arrows not showing any specific energy represent potentially not activated rotations. All values are expressed in kJ mol^{-1}. Numbers in parentheses are spin multiplicities. The proposed path is highlighted by green arrows.

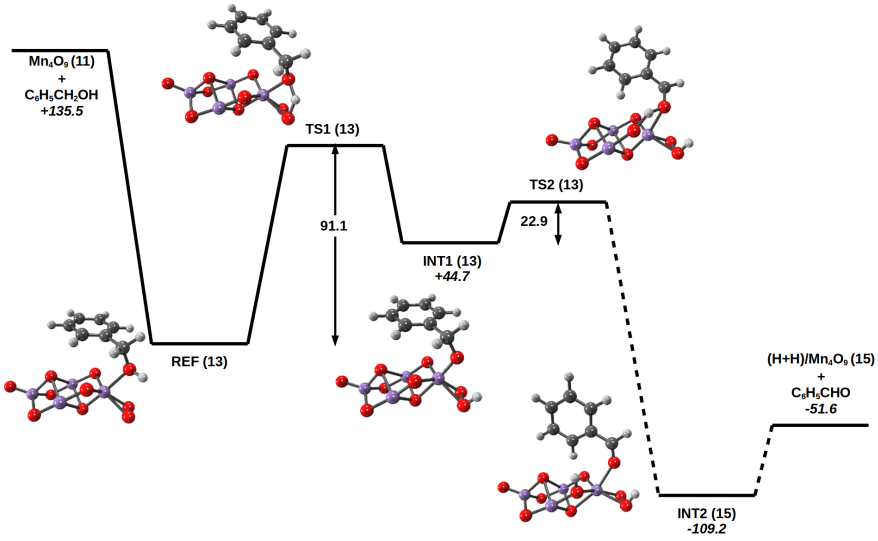

Figure 5: Oxidation of benzyl alcohol to benzaldehyde on the Mn_4O_9 catalytic cluster, occurring through the $Mn(D)_t$ mechanism. Energies of the starting reactants, minima and final products are relative to that of REF species (benzyl alcohol adsorbed on the catalytic cluster), while the energy barriers are calculated with respect to the energy of the species preceding the corresponding transition states. Spin multiplicity for each species is reported in parentheses. All values are expressed in kJ mol^{-1}. The dotted lines indicate distances not in scale.

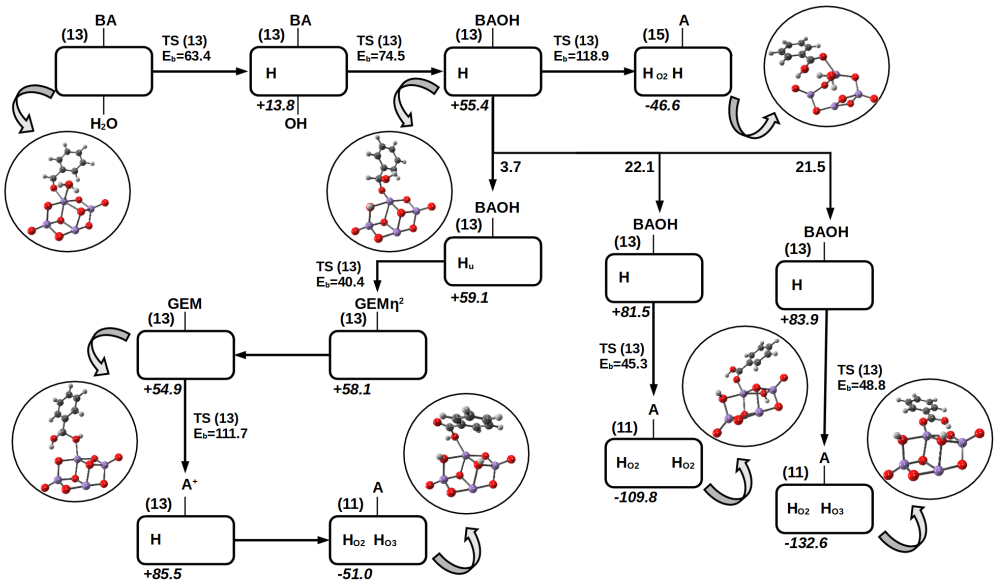

Figure 6: Proposed mechanism for benzoic acid formation. All the minimum species involved are schematically reported; for the species of peculiar interest a visual representation is also given. Energy barriers corresponding to the transition states and energies of all minima with respect to the species from which the mechanism begins (taken as reference) are indicated. All values are expressed in kJ mol^{-1}. Arrows without any specific energetics represent potentially not activated rotations. The numbers in parentheses are the spin multiplicities. The rectangle represents the Mn_4O_8 fragment, ϕCHO is the benzaldehyde, therefore ϕC(OH)HO is the oxydrilated benzaldehyde, that is the benzaldehyde with one OH moiety bonded, ϕCOOH is the benzoic acid and $\phi C(OH)_2$ the gem-diol. Hs inside the rectangles indicate hydrogen atoms directly interacting with the Mn_4O_8 cluster; the subscripts of H, u, O2 and O3, when present, indicate that the corresponding hydrogen is in the order pointing upward or bonded to either O2 or O3 oxygen sites.

List of Tables

Table 1: Significant structural descriptors, namely bond distances and dihedral angles, characterizing the benzyl alcohol adsorption on the Mn_4O_9 catalytic fragment

Distance/Å	**Mn(D)**$_t$	**Mn(D)**$_d$
Mn(D)−C_6H_5[a]	4.04	2.49
Mn(D)−Od′	2.03	2.07
Mn(D)−Od′′	2.04	1.97
Mn(D)−O	2.12	2.24
O−H	0.97	0.97
O−CH_2	1.47	1.44
Dihedral angle/°	**Mn(D)**$_t$	**Mn(D)**$_d$
Θ(O-C-C-C)	-68.9	-22.5

[a] The C_6H_5−Mn(D) distance is taken between the Mn(D) site of the Mn_4O_9 cluster and the nearest carbon atom belonging to the phenyl fragment.

Table 2: Significative pathway mechanisms (M) reported in different figures of the here work and involved in the oxidation of benzyl alcohol, benzaldehyde and carbon monoxide with their corresponding reaction rates (s) at 343 K

Pathway Mechanism	**Reference Figure**	**s/s^{-1}**
M1[a]	1	$9.4 \cdot 10^{-5}$
M2[b]	1	$5.9 \cdot 10^{-6}$
M3[c]	1	$3.6 \cdot 10^{-23}$
M4[c] (green pathway)	4	$8.7 \cdot 10^{-11}$
M5[c]	5	$9.4 \cdot 10^{-2}$
M6[d] (pathway ending with H atoms on O2 and O2)	6	$3.8 \cdot 10^{-17}$
M7[d] (pathway ending with H atoms on O2 and O3)	6	$1.4 \cdot 10^{-15}$
M8[d] (gem-diol pathway, ending with H atoms on O2 and O3)	6	$1.4 \cdot 10^{-15}$
M9[e]	NA[f]	$9.5 \cdot 10^{-4}$

[a] $\Phi CH_2OH \xrightarrow{Mn_4O_8} \Phi CHO$
[b] $H_2/Mn_4O_8 + O_2 \longrightarrow H_2O + Mn_4O_9$
[c] $\Phi CH_2OH \xrightarrow{Mn_4O_9} \Phi CHO$
[d] $(\Phi CHO + H_2O)/Mn_4O_8 \longrightarrow 2\,H/Mn_4O_8 + \Phi COOH$
[e] $CO + Mn_4O_9 \longrightarrow CO_2 + Mn_4O_8$
[f] The reference figure is here not available. CO oxidation was indeed studied at the same level of calculation used for the other studied systems (see computational details section). Particulars on the process energetics and on the optimized cartesian coordinates with the absolute energies of the species involved in the CO oxidation pathway are elsewhere reported [1] by Gueci et al.